

Discrete Noise Inversion for Next-scale Autoregressive Text-based Image Editing

Quan Dao^{1†*} **Xiaoxiao He**^{1†} **Ligong Han**^{2*}
Ngan Hoai Nguyen³ **Amin Heyrani Nobari**⁴ **Faez Ahmed**⁴
Han Zhang⁵ **Viet Anh Nguyen**⁶ **Dimitris Metaxas**¹
¹Rutgers University ²Red Hat AI Innovation ³QualcommAI Research
⁴MIT ⁵ReveAI ⁶CUHK

Abstract

Visual autoregressive models (VAR) have recently emerged as a promising class of generative models, achieving performance comparable to diffusion models in text-to-image generation tasks. While conditional generation has been widely explored, the ability to perform prompt-guided image editing without additional training is equally critical, as it supports numerous practical real-world applications. This paper investigates the text-to-image editing capabilities of VAR by introducing Visual AutoRegressive Inverse Noise (VARIN), the first noise inversion-based editing technique designed explicitly for VAR models. VARIN leverages a novel pseudo-inverse function for argmax sampling, named Location-aware Argmax Inversion (LAI), to generate inverse Gumbel noises. These inverse noises enable precise reconstruction of the source image and facilitate targeted, controllable edits aligned with textual prompts. Extensive experiments demonstrate that VARIN effectively modifies source images according to specified prompts while significantly preserving the original background and structural details, thus validating its efficacy as a practical editing approach.

1 Introduction

In the era of generative AI, diffusion models [19, 46] have emerged as dominant methods in image synthesis, outperforming GANs [14] in both *unconditional* and conditional generation tasks [9], notably in text-to-image generation [41]. This success has enabled diverse practical applications, including personalization [42, 54, 26], 3D generation [36, 58], and prompt-based image editing [3, 22, 33, 61, 18, 17], underscoring their increasing popularity and utility.¹ In contrast, autoregressive models, traditionally dominant in natural language processing, have only recently gained traction in visual synthesis. Recent models such as LlamaGen [47] and MagVit-v2 [62] have optimized image tokenization and transformer architectures, achieving performance competitive with diffusion models. Furthermore, MARS [16] integrates mixtures of experts to train large-scale text-to-image autoregressive models, whereas MAR [28] removes vector quantization by leveraging diffusion-inspired training in continuous space. Despite achieving diffusion-level quality, these methods still incur significant inference costs due to dependence on output size, limiting scalability for high-resolution generation. Addressing this issue, [50] proposed next-scale prediction to substantially reduce inference time without sacrificing performance, highlighting potential future advantages of autoregressive approaches. Additionally, [48] introduced the Hybrid VAR Transformer (HART) diffusion framework, combining visual autoregressive models (VAR) with lightweight diffusion refinement, achieving comparable results to pure diffusion methods but with reduced inference time.

¹†: Equally Contribution, *: Corresponding Author



Figure 1: Qualitative performance of VARIN given diverse prompts.

This model raises further research opportunities in downstream tasks, including personalization, prompt-based image editing, and text-to-3D synthesis within VAR-based frameworks.

In this paper, we focus specifically on prompt-guided text-to-image editing within visual autoregressive models (VAR). Given a source image and a text prompt describing desired edits, the task is to modify the image according to the prompt while preserving unrelated details from the original. We observe that VAR generates the overall structure and layout at initial scales, progressively refining finer details at higher scales. As illustrated in Figure 2, editing primarily becomes necessary at middle scales, around levels 6 or 7. A straightforward baseline is **Regeneration**, which preserves tokens at initial scales and regenerates remaining scales. However, this approach inadequately retains non-target image details.

To address these limitations, we propose **Visual Autoregressive Inverse Noise (VARIN)**, the first training-free editing method designed explicitly for VAR. Inspired conceptually by noise inversion techniques in diffusion models, VARIN identifies editable noise sets capable of perfectly reconstructing the source image, enabling precise editing. While continuous autoregressive models (e.g., Gaussian-based) allow straightforward inversion through inverse transformation flows [24], discrete VAR models like [50, 48] complicate inversion due to reliance on the non-invertible argmax sampling (Gumbel-max trick). The simplest pseudo-inverse, the one-hot argmax inversion [17], produces uncontrollable noise sets, limiting precise editing capabilities. Therefore, we propose **Location-aware Argmax Inversion (LAI)**, a novel pseudo-inverse function enhancing controllability and alignment with target prompts. LAI extracts inverse noises to reconstruct source images precisely and allows adjustable bias towards preserving source details, significantly outperforming basic regeneration. Our method demonstrates editing quality on par with more complex, optimization-based test-time tuning approaches such as Null-Text Inversion, without requiring additional retraining or intricate cross-attention manipulations. These advanced methods remain complementary and could be combined in future work for further improvements. We summarize our contributions as follows:

- We introduce first editing technique for VAR named VARIN. Our VARIN is based on noise inversion technique to obtain set of editable noises and control these noises for editing image.
- We propose Location-aware Argmax Inversion (LAI) as pseudo-inverse of argmax inversion. This allows us to extract inverse noises that perfectly reconstruct the source image. Furthermore, we can control the bias information of source image in extracted inverse noises, leading to better results.
- We validate the effectiveness of VARIN through experiments on text-to-image editing tasks, demonstrating their ability to align with target prompts while preserving source image details.

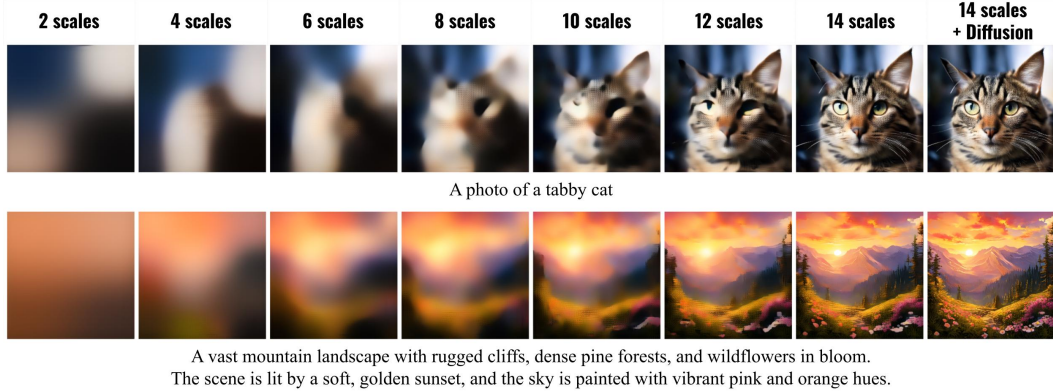


Figure 2: Visualizations of each scale of the generation process of HART [48]. The features of a cat (top) and the landscape (bottom) are only distinguishable above 6 scales.

2 Related Work

Visual autoregressive models. Autoregressive models have significantly shaped NLP, particularly through their next-token prediction paradigm [55, 1, 51, 8, 59, 2, 49]. This same paradigm has also proven effective in visual generation: models such as VQVAE [53, 40], VQGAN [12, 27], DALL-E [38], LlamaGen [47], and MARS [16] tokenize images for next-token prediction. While these token-based methods can match diffusion models in image quality, their inference speed often suffers because the number of tokens grows with image resolution.

Recent work shifts toward “next-scale prediction,” where models predict multiple size scales in parallel via residual quantization [27]. VAR [50] and HART [48] exemplify this approach by generating high-quality images in only a few steps. Furthermore, VAR is closely related to ImageBART [11], which applies transformers to each denoising step in multinomial diffusion [20]; one can interpret VAR similarly, but using a “blurring-to-deblurring” viewpoint.

Diffusion editing. Diffusion-based text-to-image editing has gained popularity for its flexibility and controllability [31, 22, 35, 21]. Many works rely on large-scale pretraining [63, 4, 13, 43, 65] or fine-tuning approaches [15, 66, 10, 44], where either model weights or embeddings are optimized at test time to achieve editing. Null-text Inversion [33] further refines editing control by adjusting “null” embeddings to align the reconstruction path with the source image.

Diffusion inversion. A key challenge in diffusion-based editing is extracting an internal representation from the source image so that edits can be made without losing fidelity. Continuous models often invert via deterministic or stochastic processes [7, 45, 29, 30, 60, 22], while recent research addresses discrete diffusion [17] and masked generative models [6]. These methods confirm that “diffusion inversion” can guide image editing by reconstructing the original data from a learned representation. Inspired by these, our work focuses on inverting a visual autoregressive model to enable text-driven editing while preserving source image content.

3 Preliminaries

In this section, we firstly review about the visual autoregressive model in Section 3.1. Motivating from method SDEdit [31] for diffusion, latter Section 3.2 introduces simple editing method for VAR called **Regeneration**, where we simply initialize the VAR generative process by beginning token maps r_1, r_2, \dots, r_t extracted from source image using VAR encoder and generate the rest of token maps $r_{t+1}, r_{t+2}, \dots, r_K$ following target text prompt c_{tgt} . Although this technique produces a fairly good final image that has the same structure as the source image and follows the target text prompt c_{tgt} , they lose background details as the final token maps are completely generated without any constraint from the source image.

3.1 Visual Autoregressive Model

VAR has a Variational AutoEncoder (VAE) based on VQ-VAE with $[C] = \{1, \dots, C\}$ of vocal size C . In training process, given an image $I \in \mathbb{R}^{3 \times H \times W}$, the VAR-VAE encoder \mathcal{E}_{VAR} will output the image into K token maps, $(r_1, r_2, \dots, r_K) = \mathcal{E}_{\text{VAR}}(I)$, where each token maps r_k has different resolution $h_k \times w_k$ and these resolution increases with the scale k . The VAR-AutoRegressive model θ can now be considered as the next scale predictor, which models the following likelihood:

$$p_{\theta}(r_1, r_2, \dots, r_K) = \prod_{k=1}^K p_{\theta}(r_k | r_1, r_2, \dots, r_{k-1}), \quad (1)$$

where $r_K \in [C]^{h_K \times w_K}$ is the token map at scale K , and the sequence $(r_1, r_2, \dots, r_{K-1})$ is the prefix of r_K . In inference time, we use VAR-AutoRegressive to predict the sequence r_1, r_2, \dots, r_K iteratively. We then pass the sequence to the VAR-VAE decoder \mathcal{D}_{VAR} to construct the generative RGB images $I_{\text{gen}} = \mathcal{D}_{\text{VAR}}(r_1, r_2, \dots, r_K)$.

Unlike traditional autoregressive methods, which flatten the image following a predefined scanning order then perform the next token prediction, the next scale prediction of VAR strictly follows the autoregressive’s behaviour. In VAR, each token map r_k depends only on the previous token maps $r_{<k}$. As a consequence, VAR costs shorter inference time than diffusion and traditional next-token prediction autoregressive models since they only need to run model for only few scale prediction ($K \approx 14$) instead of diffusion and vanilla autoregressive with thousands of model iterations.

3.2 Text-based Image Editing & Baseline Regeneration

Text-based Image Editing: We consider the text-based editing problem for the text-to-image VAR model. Given a source image $I_{\text{src}} \in \mathbb{R}^{3 \times H \times W}$ and a target prompt c_{tgt} , we want to edit the source image I_{src} to comply with the prompt c_{tgt} . In our proposed VARIN in Section 4, we use inversion algorithm for editing. Therefore, we need to define a corresponding source text c_{src} which aligns with source image for noise extraction. The inverse noises are then used for editing process with target prompt c_{tgt} as shown in Section 4.3. The image editing is evaluated based on two main criteria, which could be conflicting: the edited image should be **aligned with the target prompt** while still **preserve the unedited part from the source image**.

Baseline Regeneration: Using the VAR encoder, we could obtain the following token maps $(r_1, r_2, \dots, r_K) = \mathcal{E}_{\text{VAR}}(I_{\text{src}})$. As illustrated in Figure 2, while the token map of the beginning scales builds up the structure and layout of images, the later token map adds more detailed information. For editing with diffusion model, SDEdit [31] starts denoising generative process from middle noise level with some guidance to perform editing, while keeping the overall structure of the source image. Motivating from SDEdit, we could pick a scale index s between 1 and K , then we fix the token maps for the beginning scales from r_1, \dots, r_s , and start to generate r_{s+1}, \dots, r_K conditioning on the target prompt c_{tgt} . We name this intuitive editing method **Regeneration**, and outline it in Algorithm 4.

By keeping the beginning scale token map of the source image, the editing output image I_{tgt} could keep the overall structure and layout of the source image. However, it may fail miserably to preserve the fine-grained details in background that should not be edited, examples of failures are shown in Figure 4. To search for a more fine-grained editing control, we approach the noise inversion technique and investigate how to control the inverse noise for editing in next section.

4 Inverse Autoregressive Transformation and Editable Inverse Noise

We introduce our technique **Visual Autoregressive Inverse Noise (VARIN)** that could preserve better the unedited part of the source image. Towards this goal, we discuss the process of noise inversion for an autoregressive model in Section 4.1. For discrete space, there is no closed-form solution for inversion due to argmax operator, we therefore propose pseudo-inverse function for the argmax operator to obtain inverse noises from source image in Section 4.2. Finally, we propose the inverse noise editing algorithm for text-based image editing. The overall pipeline is in Figure 3.

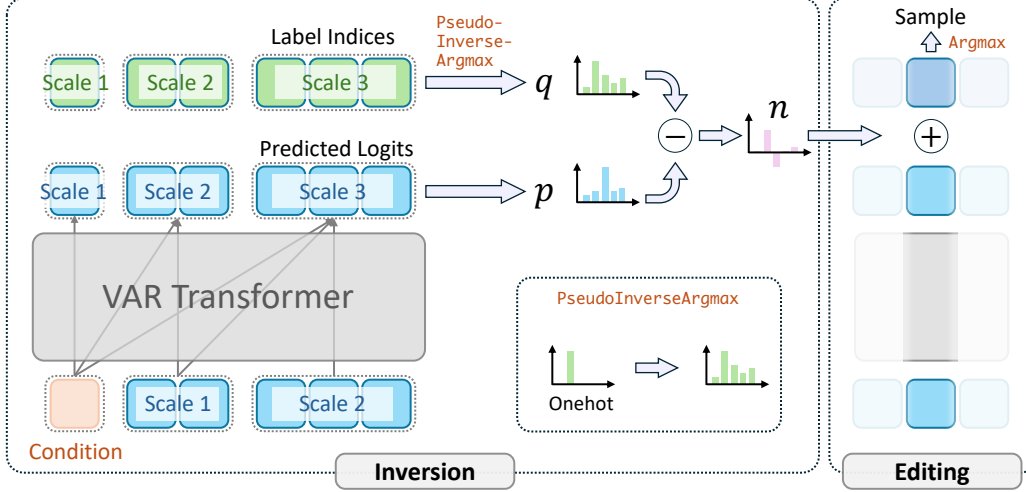


Figure 3: VARIN pipeline: the prefix token $c_{src} + r_{<k}$ is fed to transformer to get log probability p_k . We then use pseudo inverse-argmax to find the inverse noise n_k from ground truth label r_k and logit p_k . These noise set n_1, n_2, \dots, n_K is later used for editing control.

4.1 Discrete Inverse Autoregressive Transformations

Given a continuous Gaussian autoregressive model $p_\theta(x_t|x_{<t})$ and a sequence of tokens $\{x_1, x_2, \dots, x_T\}$, we could apply an inverse transformation in parallel to find the sequence of inverse noises that perfectly reconstruct the sequence [24]. To see this, note that under the Gaussian assumption of $p_\theta(x_t|x_{<t})$, we have $x_t = \mu_t + \sigma_t \odot \epsilon_t$, where μ_t and $\sigma_t > 0$ are the conditional mean and standard deviation of x_t given the history $x_{<t}$. We can obtain ϵ_t by $\epsilon_t = \frac{x_t - \mu_t}{\sigma_t}$. Computing the inverse noise under the Gaussian case could be implemented in parallel due to the independence of ϵ_t and $\epsilon_{t'}$ over different time stamps $t \neq t'$. The above inversion only holds when the noise admits a continuous density. Unfortunately, most of autoregressive generative models for vision including VAR are based on discrete tokens and model the sequence of token with multinomial distribution. Consequentially, the inversion could no longer be straightforwardly integrated into the VAR pipeline.

We now propose a pseudo-inversion for VAR models that extends the continuous noise inversion to the case of *discrete* tokens. The VAR models use a multinomial distribution, where samples are drawn using the Gumbel-max trick. A Gumbel distribution with mean 0 and scale 1 has a continuous density $\exp(-z + \exp(-z))$ for any value z . We consider the discrete inverse autoregressive transformation problem using the Gumbel-max trick as follows:

$$\begin{aligned} p_t &\leftarrow p_\theta(\cdot|r_{<t}) \\ \text{Find Gumbel noise } n_t \text{ s.t. } \text{argmax}(p_t + n_t) &= r_t, \end{aligned} \quad (2)$$

with (unnormalized) log probability $p_t \in \mathbb{R}^{l \times C}$, n_t is the Gumbel noise from Gumbel-max trick, and $r_t \in \mathbb{R}^l$ is the ground truth label with l is number of tokens. As shown in Equation (2), there is no perfect way to obtain the reverse Gumbel noise from a label and predicted probability, as the Gumbel-max trick involves **an argmax operator**, which is apparently **non-invertible**. Therefore, in the next section, we propose two pseudoinverse functions for the argmax operator in Section 4.2.

4.2 Pseudo-inverse Argmax

Since $(p_t + n_t)$ represents the Gumbel-perturbed logits, we need to choose the unnormalized log probability q_t such that $q_t = p_t + n_t$ and $\text{argmax}(q_t) = r_t$. Notably, to ensure the editing ability, we better need the n_t to follow the below properties:

- **Prop 1:** n_t needs to be likely sampled from standard Gumbel noise since in line 6 of Algorithm 3, we interpolate n_t with standard Gumbel noise for preserving randomness of generative process.
- **Prop 2:** n_t needs to preserve some bias information from source image. This allows the editing algorithm to preserve the unedited part from source image.

Now, we discuss about how to choose pseudoinverse function for argmax operator. The easiest way is setting $q_t = \text{LogOnehot}(r_t)$, and we call this **Onehot Argmax Inversion (OAI)**. With OAI, we can

Algorithm 1 Location-aware Argmax Inversion Function (LAI)

Input: tokens $r \in [C]^l$, log probability $p \in \mathbb{R}^{l \times C}$, and information preserving term τ

- 1: $r_{\text{mask}} \leftarrow \text{Onehot}(r, \text{num_classes} = C)$
 $\in \mathbb{R}^{l \times C}$
- 2: $l_{\text{max}} \leftarrow \text{Sum}(r_{\text{mask}} \odot p, \text{dim} = -1)$ $\triangleright \in \mathbb{R}^{l \times 1}$
- 3: $q_{\text{max}} \sim \text{Gumbel}(\mu = l_{\text{max}}, \beta = 1)$ $\triangleright \in \mathbb{R}^{l \times 1}$
- 4: $q \sim \text{GumbelTrunc}(\mu = p, \beta = 1, \text{trunc} = q_{\text{max}} - \tau)$ $\triangleright \in \mathbb{R}^{l \times C}$. See Algorithm 5
- 5: $q \leftarrow q \odot (1 - r_{\text{mask}}) + q_{\text{max}} \odot r_{\text{mask}}$ $\triangleright \in \mathbb{R}^{l \times C}$

Output: q

Algorithm 2 Visual Autoregressive Inverse Noise (VARIN)

Input: Source image I_{src} , text prompt c_{tgt}

Parameters: τ

Parallel Autoregressive Inversion:

- 1: $(r_1, r_2, \dots, r_K) \leftarrow \mathcal{E}_{\text{VAR}}(I_{\text{src}})$
- 2: **for** t from 1 to K **do** \triangleright logits
- 3: $q_t \leftarrow \text{LAI}(r_t, p_t)$ \triangleright Pseudo-inverse argmax Algorithm 1
- 4: $n_t \leftarrow q_t - p_t$ \triangleright Gumbel noise inversion
- 5: **end for**

Return: (n_1, n_2, \dots, n_K)

find the list of inverse noise for perfect reconstruction. However, when using inverse noise OAI for editing, it usually fails to control the editing process. The reason is that the q_t is 0 at the label index and significantly negative at other indices. This results in $n_t = q_t - p_t$ not likely being sampled from a standard Gumbel noise distribution violating **Prop 1** and n_t will be highly biased by source image since q_t is extremely biased by label of token. Therefore, in editing, it is hard to control the editing process with OAI. Furthermore, we notice that the OAI process relies only on ground-truth labels and omits the information of predicted logits p_t from models.

To remedy the above issues, we propose a novel argmax inversion function called **Location-aware Argmax Inversion (LAI)**. Since $q_t = p_t + n_t$ and n_t is sampled from standard Gumbel noise, q_t should be close to p_t . LAI exploits this property, and it takes p_t as the location of Gumbel-max sampling. This makes q_t closer to p_t , and n_t is more likely sampled from standard Gumbel distribution which is then satisfied **Prop 1**. For the remaining discussion, we will omit subscript t to avoid clutter notation. To ensure the argmax condition, for each token i from 1 to l , the ground truth label is $r[i]$, we sample $q[i]$ so that $\text{argmax}(q[i]) = r[i]$. Firstly, we sample the value for $q[i]_{r[i]}$ using the Gumbel-max trick with the predicted location $p[i]_{r[i]}$. Later, we sample other position $q[i]_{\neq r[i]}$ by truncated Gumbel-max trick with corresponding predicted location and truncated value $q[i]_{r[i]} - \tau$. Please noted that τ is very important parameter to control the unedited part preservation and we shall discuss details of τ below.

Hyperparameter τ in LAI: When $\tau = 0$, the n_t from LAI satisfies **Prop 1** but it still fails to edit while preserving the background. We could explain this effect: For simplicity, we consider $q \in \mathbb{R}^C$ is a vector. When $\lambda = 0$, the q sampled from Algorithm 5 (Gumbel Trunc) is highly uncertain cause there exist some indices j such that $q_j \approx q_i$, where $i = \text{argmax}_k q_k$. Therefore, during editing, $q^{\text{edit}} = p + (1 - \lambda) \cdot g + \lambda \cdot n = p + n + (1 - \lambda) \cdot (g - n) = q + (1 - \lambda) \cdot (g - n) = q + \epsilon$. Since q is highly sensitive, even a small ϵ can cause a change in the maximum index of q^{edit} , such that $\text{argmax}_k q_k^{\text{edit}} = j$. As a result, preserving the unedited part becomes exceedingly difficult. Therefore, by setting τ , we could let q_t retains bias from source image which provides useful information to n_t and control the sensitivity of Algorithm 3 better. This is also satisfied **Prop 2**.

The efficient implementation is shown in Algorithm 1. LAI always guarantees perfect reconstruction, the same as OAI, but q_t is closer to p_t , and n_t is more like standard Gumbel, which satisfied both above noise properties. We use LAI in Line 3 of Algorithm 2.

4.3 Editing with VARIN

For editing using inversion, similar to Regeneration Editing, we first obtain the token maps for each scale using the VAR encoder. We then use Algorithm 2 to collect the list of inverse noise n_1, n_2, \dots, n_K . For each t , we get the predicted log probability p_t from autoregressive model p_θ . Instead of sampling using the Gumbel-max trick given p_t as in Algorithm 4, which uses new Gumbel noise g , we interpolate new

Algorithm 3 Editing by VARIN

Input:

- 1: $(r_1, r_2, \dots, r_K) \leftarrow \mathcal{E}_{\text{VAR}}(I_{\text{src}})$
- 2: $n_1, n_2, \dots, n_K \leftarrow \text{VARIN}((r_1, r_2, \dots, r_K), c_{\text{src}})$
- 3: **for** t from s to K **do** $\triangleright s$ is staring scale
- 4: $p_t \leftarrow p_\theta(\cdot | r_{<t}, c_{\text{tgt}})$ $\triangleright p_t$ is log probability
- 5: $g \sim \text{Gumbel}(0, I)$
- 6: $q_t = p_t + (1 - \lambda) \cdot g + \lambda n_t$
- 7: $\tilde{r}_t = \text{argmax}(q_t)$
- 8: **end for**
- 9: $I_{\text{tgt}} \leftarrow \mathcal{D}_{\text{VAR}}(r_1, \dots, r_{s-1}, \tilde{r}_s, \dots, \tilde{r}_K)$

Output: I_{tgt}

Table 1: We evaluate our method VARIN against discrete generative model such as DICE and EditAR. We can see that our method outperforms DICE in terms of editing part with better CLIP Similarity but slightly underperforms in terms of background preservation due to the T2I reconstruction ability. With EditAR, we are better in terms of background reconstruction. Compared to recent continuous diffusion, we also achieve on par performance.

Method		Structure		Background Preservation			CLIP Similarity		
Name	T2I	Distance $\times 10^3\downarrow$	PSNR \uparrow	LPIPS $\times 10^3\downarrow$	MSE $\times 10^4\downarrow$	SSIM $\times 10^2\uparrow$	Whole \uparrow	Edited \uparrow	
Continuous	Prompt-to-Prompt	SD1.4	69.43	17.87	208.80	219.88	71.14	25.01	22.44
	Negative Prompt	SD1.4	16.17	26.21	69.01	39.73	83.40	24.61	21.87
	PnP Inversion	SD1.4	11.65	27.22	54.55	32.86	84.76	25.02	22.10
	Null-text Inversion	SD1.4	13.44	27.03	60.67	35.86	84.11	24.75	21.86
	Pix2pix-zero	SD1.4	61.68	20.44	172.22	144.12	74.67	22.80	20.54
	MasaCtrl	SD1.4	28.38	22.17	106.62	86.97	79.67	23.96	21.16
	InfEdit	SD1.4	14.22	27.52	47.98	34.17	85.05	24.89	22.03
	InstructPix2Pix	SD1.5	107.43	16.69	271.33	392.22	68.39	23.49	22.20
	MGIE	SD1.5	67.41	21.20	142.25	295.11	77.52	24.28	21.79
	DDPM-Inversion	SD1.4	22.12	22.66	67.66	53.33	78.95	26.22	23.02
Discrete	DICE	Paella	11.34	27.29	52.90	43.76	89.79	23.79	21.23
	EditAR	LlamaGen	39.43	21.32	117.15	130.27	75.13	24.87	21.87
	Regeneration	HART	25.56	20.45	106.50	95.90	73.31	24.65	21.13
	VARIN	HART	<u>11.46</u>	<u>26.54</u>	<u>54.04</u>	38.33	<u>85.39</u>	25.05	<u>21.49</u>

noise g with inverse noise n_t by interpolation coefficients λ . The λ is hyperparameter for tuning the editing process.

5 Experiments

In this section, we first provide details of the evaluation dataset for text-based image editing task in Section 5. Section 5.1 presents the reconstruction performance of our proposed method, VARIN + HART. Later, in Section 5.2, we conduct editing experiments to demonstrate that VARIN can effectively do text-based image editing. Due to limited space, ablation is put in appendix.

Dataset: To conduct the experiment, we use the Prompt-based Image Editing Benchmark (PIE-Bench) [23] which is a dataset created to evaluate text-to-image (T2I) editing methods. It includes 700 images in 9 different editing scenarios, making it a useful evaluation protocol for testing how well these methods handle text-guided image edits. The dataset contains detailed annotations and variety of tasks for us to thoroughly test and fairly compare our method with other approaches.

5.1 Inversion Reconstruction

Here we evaluate the reconstruction performance of our inversion method, VARIN. First, we use Algorithm 2 to generate a set of inverse noises. These inverse noises are then used to reconstruct token maps at each scale. Finally, the final token maps are decoded back to images.

Table 2: Inversion reconstruction performance among discrete generative model. This indicates the underperformance of HART compared to Paella in terms of reconstruction.

Method		Metric			
Inversion	Model	PSNR \uparrow	LPIPS $\times 10^3 \downarrow$	MSE $\times 10^4 \downarrow$	SSIM $\times 10^2 \uparrow$
DICE	Paella	30.91	39.81	11.07	90.22
VARIN	HART	26.00	70.26	33.20	79.83

Evaluation Metrics. To measure the reconstruction, we adopt image similarity metric such as Peak Signal-to-Noise Ratio (PSNR), Learned Perceptual Image Patch Similarity (LPIPS) [64], Mean Squared Error (MSE), and Structural Similarity Index Measure (SSIM) [57] to compute the difference between source images and the reconstructed images.

Results. In Table 2, we compares our inversion VARIN with DICE [17], as both operate on discrete distributions. While DICE is based on a discrete diffusion model, our approach utilizes HART, a discrete visual autoregressive model. Mathematically, discrete noise inversion for both DICE and VARIN should produce token maps identical to the input token maps. However, the recorded metrics reveal a gap between the reconstructed images and the original source images. This discrepancy

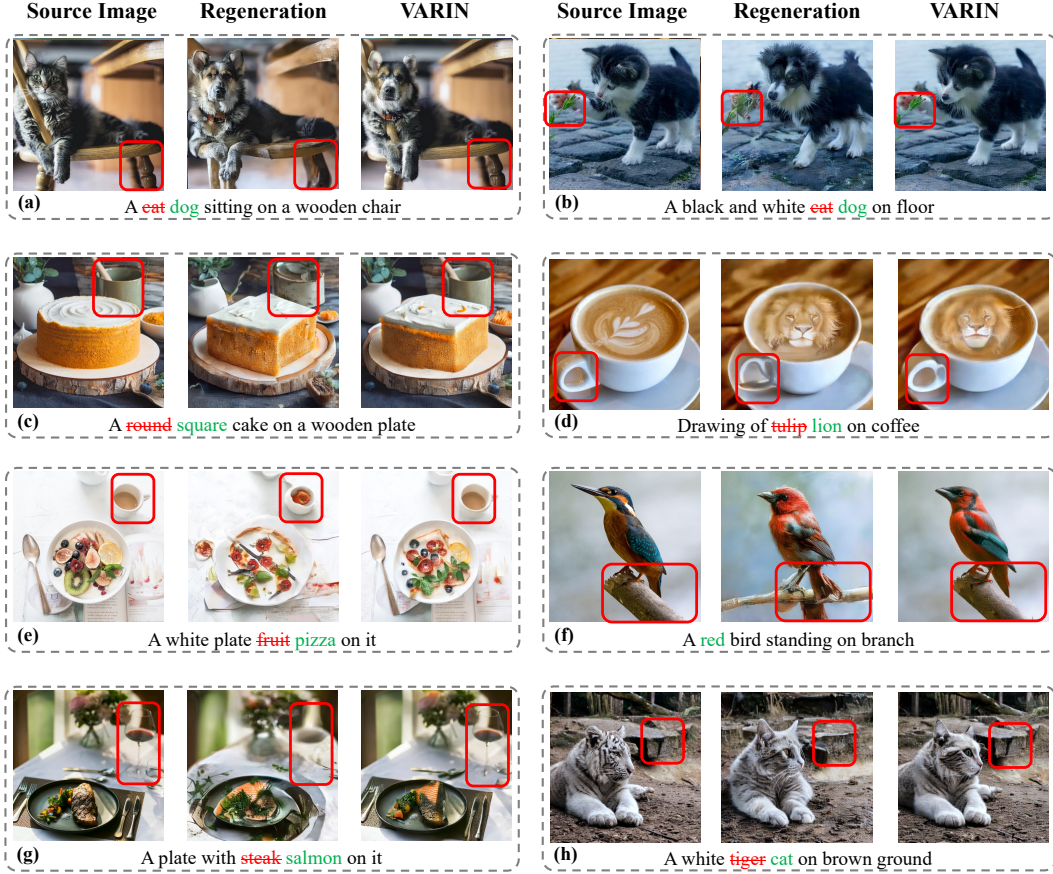


Figure 4: Qualitative result of editing results between VARIN and baseline Regeneration. We should better editing capability and background preservation.

arises because both Paella [39] and HART rely on vector quantization autoencoders, which inherently involve reconstruction loss due to compression. From Table 2, we observe that the VAR-VAE of HART underperforms compared to the VQ-VAE used in Paella.

5.2 Text-based Image Editing Performance

This section demonstrates the effectiveness of our editing algorithm VARIN. For both Regeneration and VARIN, by default, we set the start scale of editing $s = 6$ based on observation from Figure 2 and set the τ to be 18 in LAI. Furthermore, we propose a linear scheduler for λ with respect to scale, where $\lambda = 1$ on scale s and start reducing linearly to 0 at final scale 14.

Evaluation Metrics. We evaluate the performance of our proposed editing methods on three main aspects: structural similarity, background preservation, and alignment between the edit prompt and the generated image. To assess structural similarity between the original and generated images, we apply the structure distance metric from [52]. For evaluating background preservation outside the editing mask, we use PSNR, LPIPS, MSE, and SSIM. Consistency between the edit prompt and the generated image is measured using the CLIP Similarity Score [37], computed for the entire image and specifically for the regions within the editing mask. These metrics offer a holistic assessment of our inversion method, addressing methods ability to maintain structure, preserve background details, and ensure prompt-image consistency, as in [23].

Results. Looking at Table 1, we begin by fairly comparing our editing method, VARIN, with training- and optimization-free approaches including Regeneration, DICE, and DDPM-Inversion, as VARIN similarly relies solely on an instant inversion technique. While VARIN outperforms DICE in editing effectiveness, it exhibits marginally lower preservation performance, likely due to HART’s weaker



Figure 5: Fine-grained editing examples with VARIN using Switti [56]. VARIN successfully performs localized modifications such as changing facial expressions, object replacement, and hand gestures while preserving original image details.

reconstruction capability compared to Paella (see Section 5.1). Methodologically, VARIN is based on a next-scale autoregressive framework, whereas DICE adopts a discrete diffusion approach. Since the editing quality in both methods is closely tied to the sampling process, it is worth noting that VARIN requires only 10 sampling steps, while diffusion-based methods like DICE demand more, resulting in slower inference. Empirically, VARIN achieves real-time editing at approximately 1 second per image, compared to 2 seconds for DICE. Against DDPM-Inversion and Regeneration (see Figure 4 and Figure 10 in Supplementary Materials for qualitative comparisons with Regeneration), VARIN provides better reconstruction fidelity and background retention, while also adhering to the target prompt more effectively. In terms of efficiency, VARIN is approximately $10\times$ faster than DDPM-Inversion. Overall, among purely training-free editing methods, VARIN achieves competitive quantitative performance while substantially outperforming other diffusion based-approaches in editing speed. Secondly, within the category of autoregressive editing, we compare VARIN to the recently proposed EditAR model [34]. VARIN achieves superior performance across most evaluation metrics, with the exception of CLIP Edited Similarity. Unlike EditAR, which requires additional training akin to InstructPix2Pix [4], VARIN relies solely on an inversion-based approach using next-scale autoregressive prediction, and does not require any task-specific fine-tuning.

In comparison to continuous diffusion-based editing techniques such as MasaCtrl [5], MGIE [13], InstructPix2Pix [4], Prompt-to-Prompt [18], and Pix2Pix-Zero [38], VARIN demonstrates superior background and structural preservation. It achieves a better balance between editing precision and content fidelity. This balance is also comparable to that of more advanced editing methods including InfEdit, PnP Inversion, Null-text Inversion, and Negative Prompting [32]. Unlike these diffusion-based methods, VARIN enables real-time editing with an average inference time of approximately 1 second per image, leveraging instant inversion and next-scale autoregressive. In contrast, approaches such as Negative Prompting and Null-text Inversion often require time-consuming optimization during both inversion and editing stages. Other techniques like PnP and InfEdit depend on pretrained editing models (e.g., P2P) or attention manipulation, whereas VARIN is entirely training-free. While attention control and pretrained editing models offer promising directions, they are orthogonal to our approach and can be integrated with VARIN. We leave such extensions for future work.

As demonstrated in Figure 1, VARIN effectively handles diverse prompts to add objects, change backgrounds, and alter image styles. These edits maintain alignment with the target prompts while preserving essential background details. Additionally, fine-grained editing results using the base model Switti [56] are presented in Figure 5, illustrating moderate local edits like closing eyes, turning heads, changing objects (e.g., book to iPad), and adjusting hand gestures or leg positions, though substantial pose or structural modifications remain challenging. In addition to the automated evaluations, we conducted a user study to assess and compare the visualization quality and editing prompt agreement of DDPM-Inv, DICE, and VARIN methods (detailed in Table 6 within the supplementary materials).

6 Conclusion

We proposed VARIN, that enable text-guided image editing capabilities for the text-to-image VAR (HART). Through extensive experiments, we have shown that this method successfully perform

text-guided image editing while maintaining background preservation. These editing advancements extend HART’s capabilities beyond mere text-to-image generation, making it a more versatile tool for real-world applications. Moving forward, promising directions for future research include exploring the application of VARIN to other traditional next-token autoregressive models or investigating attention control like [18] to further improve editing quality.

References

- [1] J. Achiam, S. Adler, S. Agarwal, L. Ahmad, I. Akkaya, F. L. Aleman, D. Almeida, J. Altenschmidt, S. Altman, S. Anadkat, et al. Gpt-4 technical report. *arXiv preprint arXiv:2303.08774*, 2023.
- [2] J. Bai, S. Bai, Y. Chu, Z. Cui, K. Dang, X. Deng, Y. Fan, W. Ge, Y. Han, F. Huang, et al. Qwen technical report. *arXiv preprint arXiv:2309.16609*, 2023.
- [3] M. Brack, F. Friedrich, K. Kornmeier, L. Tsaban, P. Schramowski, K. Kersting, and A. Passos. Ledit++: Limitless image editing using text-to-image models. In *Proceedings of the IEEE/CVF Conference on Computer Vision and Pattern Recognition (CVPR)*, 2024.
- [4] T. Brooks, A. Holynski, and A. A. Efros. Instructpix2pix: Learning to follow image editing instructions. In *Proceedings of the IEEE/CVF Conference on Computer Vision and Pattern Recognition*, pages 18392–18402, 2023.
- [5] M. Cao, X. Wang, Z. Qi, Y. Shan, X. Qie, and Y. Zheng. Masactrl: Tuning-free mutual self-attention control for consistent image synthesis and editing. In *Proceedings of the IEEE/CVF International Conference on Computer Vision (ICCV)*, pages 22560–22570, October 2023.
- [6] H. Chang, H. Zhang, L. Jiang, C. Liu, and W. T. Freeman. Maskgit: Masked generative image transformer. In *Proceedings of the IEEE/CVF Conference on Computer Vision and Pattern Recognition*, pages 11315–11325, 2022.
- [7] R. T. Chen, Y. Rubanova, J. Bettencourt, and D. K. Duvenaud. Neural ordinary differential equations. *Advances in neural information processing systems*, 31, 2018.
- [8] A. Chowdhery, S. Narang, J. Devlin, M. Bosma, G. Mishra, A. Roberts, P. Barham, H. W. Chung, C. Sutton, S. Gehrmann, et al. Palm: Scaling language modeling with pathways. *Journal of Machine Learning Research*, 24(240):1–113, 2023.
- [9] P. Dhariwal and A. Nichol. Diffusion models beat gans on image synthesis. *Advances in neural information processing systems*, 34:8780–8794, 2021.
- [10] W. Dong, S. Xue, X. Duan, and S. Han. Prompt tuning inversion for text-driven image editing using diffusion models. In *Proceedings of the IEEE/CVF International Conference on Computer Vision*, pages 7430–7440, 2023.
- [11] P. Esser, R. Rombach, A. Blattmann, and B. Ommer. Imagebart: Bidirectional context with multinomial diffusion for autoregressive image synthesis. *Advances in neural information processing systems*, 34:3518–3532, 2021.
- [12] P. Esser, R. Rombach, and B. Ommer. Taming transformers for high-resolution image synthesis. In *Proceedings of the IEEE/CVF conference on computer vision and pattern recognition*, pages 12873–12883, 2021.
- [13] T.-J. Fu, W. Hu, X. Du, W. Y. Wang, Y. Yang, and Z. Gan. Guiding instruction-based image editing via multimodal large language models. *arXiv preprint arXiv:2309.17102*, 2023.
- [14] I. Goodfellow, J. Pouget-Abadie, M. Mirza, B. Xu, D. Warde-Farley, S. Ozair, A. Courville, and Y. Bengio. Generative adversarial nets. *Advances in neural information processing systems*, 27, 2014.
- [15] L. Han, Y. Li, H. Zhang, P. Milanfar, D. Metaxas, and F. Yang. Svdiff: Compact parameter space for diffusion fine-tuning. In *Proceedings of the IEEE/CVF International Conference on Computer Vision*, pages 7323–7334, 2023.
- [16] W. He, S. Fu, M. Liu, X. Wang, W. Xiao, F. Shu, Y. Wang, L. Zhang, Z. Yu, H. Li, et al. Mars: Mixture of auto-regressive models for fine-grained text-to-image synthesis. *arXiv preprint arXiv:2407.07614*, 2024.
- [17] X. He, L. Han, Q. Dao, S. Wen, M. Bai, D. Liu, H. Zhang, M. R. Min, F. Juefei-Xu, C. Tan, et al. Dice: Discrete inversion enabling controllable editing for multinomial diffusion and masked generative models. *arXiv preprint arXiv:2410.08207*, 2024.

- [18] A. Hertz, R. Mokady, J. Tenenbaum, K. Aberman, Y. Pritch, and D. Cohen-Or. Prompt-to-prompt image editing with cross attention control. *arXiv preprint arXiv:2208.01626*, 2022.
- [19] J. Ho, A. Jain, and P. Abbeel. Denoising diffusion probabilistic models. *Advances in neural information processing systems*, 33:6840–6851, 2020.
- [20] E. Hogeboom, D. Nielsen, P. Jaini, P. Forré, and M. Welling. Argmax flows and multinomial diffusion: Learning categorical distributions. *Advances in Neural Information Processing Systems*, 34:12454–12465, 2021.
- [21] Y. Huang, J. Huang, Y. Liu, M. Yan, J. Lv, J. Liu, W. Xiong, H. Zhang, S. Chen, and L. Cao. Diffusion model-based image editing: A survey. *arXiv preprint arXiv:2402.17525*, 2024.
- [22] I. Huberman-Spiegelglas, V. Kulikov, and T. Michaeli. An edit friendly ddpn noise space: Inversion and manipulations. In *Proceedings of the IEEE/CVF Conference on Computer Vision and Pattern Recognition*, pages 12469–12478, 2024.
- [23] X. Ju, A. Zeng, Y. Bian, S. Liu, and Q. Xu. Direct inversion: Boosting diffusion-based editing with 3 lines of code. *arXiv preprint arXiv:2310.01506*, 2023.
- [24] D. P. Kingma, T. Salimans, R. Jozefowicz, X. Chen, I. Sutskever, and M. Welling. Improved variational inference with inverse autoregressive flow. *Advances in Neural Information Processing Systems*, 29, 2016.
- [25] W. Kool, H. Van Hoof, and M. Welling. Stochastic beams and where to find them: The gumbel-top-k trick for sampling sequences without replacement. In *International Conference on Machine Learning*, pages 3499–3508. PMLR, 2019.
- [26] N. Kumari, B. Zhang, R. Zhang, E. Shechtman, and J.-Y. Zhu. Multi-concept customization of text-to-image diffusion. In *CVPR*, 2023.
- [27] D. Lee, C. Kim, S. Kim, M. Cho, and W.-S. Han. Autoregressive image generation using residual quantization. In *Proceedings of the IEEE/CVF Conference on Computer Vision and Pattern Recognition*, pages 11523–11532, 2022.
- [28] T. Li, Y. Tian, H. Li, M. Deng, and K. He. Autoregressive image generation without vector quantization. *arXiv preprint arXiv:2406.11838*, 2024.
- [29] Y. Lipman, R. T. Chen, H. Ben-Hamu, M. Nickel, and M. Le. Flow matching for generative modeling. *arXiv preprint arXiv:2210.02747*, 2022.
- [30] X. Liu, C. Gong, and Q. Liu. Flow straight and fast: Learning to generate and transfer data with rectified flow. *arXiv preprint arXiv:2209.03003*, 2022.
- [31] C. Meng, Y. He, Y. Song, J. Song, J. Wu, J.-Y. Zhu, and S. Ermon. Sdedit: Guided image synthesis and editing with stochastic differential equations. *arXiv preprint arXiv:2108.01073*, 2021.
- [32] D. Miyake, A. Iohara, Y. Saito, and T. Tanaka. Negative-prompt inversion: Fast image inversion for editing with text-guided diffusion models. *arXiv preprint arXiv:2305.16807*, 2023.
- [33] R. Mokady, A. Hertz, K. Aberman, Y. Pritch, and D. Cohen-Or. Null-text inversion for editing real images using guided diffusion models. In *Proceedings of the IEEE/CVF Conference on Computer Vision and Pattern Recognition*, pages 6038–6047, 2023.
- [34] J. Mu, N. Vasconcelos, and X. Wang. Editar: Unified conditional generation with autoregressive models. *arXiv preprint arXiv:2501.04699*, 2025.
- [35] T.-T. Nguyen, D.-A. Nguyen, A. Tran, and C. Pham. Flexedit: Flexible and controllable diffusion-based object-centric image editing. *arXiv preprint arXiv:2403.18605*, 2024.
- [36] B. Poole, A. Jain, J. T. Barron, and B. Mildenhall. Dreamfusion: Text-to-3d using 2d diffusion. *arXiv*, 2022.

- [37] A. Radford, J. W. Kim, C. Hallacy, A. Ramesh, G. Goh, S. Agarwal, G. Sastry, A. Askell, P. Mishkin, J. Clark, et al. Learning transferable visual models from natural language supervision. In *International conference on machine learning*, pages 8748–8763. PMLR, 2021.
- [38] A. Ramesh, M. Pavlov, G. Goh, S. Gray, C. Voss, A. Radford, M. Chen, and I. Sutskever. Zero-shot text-to-image generation. In *International conference on machine learning*, pages 8821–8831. Pmlr, 2021.
- [39] D. Rampas, P. Pernias, and M. Aubreille. A novel sampling scheme for text-and image-conditional image synthesis in quantized latent spaces. *arXiv preprint arXiv:2211.07292*, 2022.
- [40] A. Razavi, A. Van den Oord, and O. Vinyals. Generating diverse high-fidelity images with vq-vae-2. *Advances in neural information processing systems*, 32, 2019.
- [41] R. Rombach, A. Blattmann, D. Lorenz, P. Esser, and B. Ommer. High-resolution image synthesis with latent diffusion models. In *Proceedings of the IEEE/CVF conference on computer vision and pattern recognition*, pages 10684–10695, 2022.
- [42] N. Ruiz, Y. Li, V. Jampani, Y. Pritch, M. Rubinstein, and K. Aberman. Dreambooth: Fine tuning text-to-image diffusion models for subject-driven generation. In *Proceedings of the IEEE/CVF conference on computer vision and pattern recognition*, pages 22500–22510, 2023.
- [43] S. Sheynin, A. Polyak, U. Singer, Y. Kirstain, A. Zohar, O. Ashual, D. Parikh, and Y. Taigman. Emu edit: Precise image editing via recognition and generation tasks. In *Proceedings of the IEEE/CVF Conference on Computer Vision and Pattern Recognition*, pages 8871–8879, 2024.
- [44] Y. Shi, C. Xue, J. H. Liew, J. Pan, H. Yan, W. Zhang, V. Y. Tan, and S. Bai. Dragdiffusion: Harnessing diffusion models for interactive point-based image editing. In *Proceedings of the IEEE/CVF Conference on Computer Vision and Pattern Recognition*, pages 8839–8849, 2024.
- [45] J. Song, C. Meng, and S. Ermon. Denoising diffusion implicit models. In *International Conference on Learning Representations*, 2021.
- [46] Y. Song, J. Sohl-Dickstein, D. P. Kingma, A. Kumar, S. Ermon, and B. Poole. Score-based generative modeling through stochastic differential equations. *arXiv preprint arXiv:2011.13456*, 2020.
- [47] P. Sun, Y. Jiang, S. Chen, S. Zhang, B. Peng, P. Luo, and Z. Yuan. Autoregressive model beats diffusion: Llama for scalable image generation. *arXiv preprint arXiv:2406.06525*, 2024.
- [48] H. Tang, Y. Wu, S. Yang, E. Xie, J. Chen, J. Chen, Z. Zhang, H. Cai, Y. Lu, and S. Han. Hart: Efficient visual generation with hybrid autoregressive transformer. *arXiv preprint arXiv:2410.10812*, 2024.
- [49] G. Team, R. Anil, S. Borgeaud, J.-B. Alayrac, J. Yu, R. Soricut, J. Schalkwyk, A. M. Dai, A. Hauth, K. Millican, et al. Gemini: a family of highly capable multimodal models. *arXiv preprint arXiv:2312.11805*, 2023.
- [50] K. Tian, Y. Jiang, Z. Yuan, B. Peng, and L. Wang. Visual autoregressive modeling: Scalable image generation via next-scale prediction. *arXiv preprint arXiv:2404.02905*, 2024.
- [51] H. Touvron, T. Lavril, G. Izacard, X. Martinet, M.-A. Lachaux, T. Lacroix, B. Rozière, N. Goyal, E. Hambro, F. Azhar, et al. Llama: Open and efficient foundation language models. *arXiv preprint arXiv:2302.13971*, 2023.
- [52] N. Tumanyan, M. Geyer, S. Bagon, and T. Dekel. Plug-and-play diffusion features for text-driven image-to-image translation. In *Proceedings of the IEEE/CVF Conference on Computer Vision and Pattern Recognition*, pages 1921–1930, 2023.
- [53] A. Van Den Oord, O. Vinyals, et al. Neural discrete representation learning. *Advances in neural information processing systems*, 30, 2017.

- [54] T. Van Le, H. Phung, T. H. Nguyen, Q. Dao, N. N. Tran, and A. Tran. Anti-dreambooth: Protecting users from personalized text-to-image synthesis. In *Proceedings of the IEEE/CVF International Conference on Computer Vision*, pages 2116–2127, 2023.
- [55] A. Vaswani. Attention is all you need. *Advances in Neural Information Processing Systems*, 2017.
- [56] A. Voronov, D. Kuznedelev, M. Khoroshikh, V. Khrulkov, and D. Baranchuk. Switti: Designing scale-wise transformers for text-to-image synthesis. 2024.
- [57] Z. Wang, A. C. Bovik, H. R. Sheikh, and E. P. Simoncelli. Image quality assessment: from error visibility to structural similarity. *IEEE transactions on image processing*, 13(4):600–612, 2004.
- [58] Z. Wang, C. Lu, Y. Wang, F. Bao, C. Li, H. Su, and J. Zhu. Prolificdreamer: High-fidelity and diverse text-to-3d generation with variational score distillation. *arXiv preprint arXiv:2305.16213*, 2023.
- [59] B. Workshop, T. L. Scao, A. Fan, C. Akiki, E. Pavlick, S. Ilić, D. Hesslow, R. Castagné, A. S. Luccioni, F. Yvon, et al. Bloom: A 176b-parameter open-access multilingual language model. *arXiv preprint arXiv:2211.05100*, 2022.
- [60] C. H. Wu and F. De la Torre. Unifying diffusion models’ latent space, with applications to cyclediffusion and guidance. *arXiv preprint arXiv:2210.05559*, 2022.
- [61] C. H. Wu and F. D. la Torre. A latent space of stochastic diffusion models for zero-shot image editing and guidance. In *ICCV*, 2023.
- [62] L. Yu, J. Lezama, N. B. Gundavarapu, L. Versari, K. Sohn, D. Minnen, Y. Cheng, V. Birodkar, A. Gupta, X. Gu, et al. Language model beats diffusion—tokenizer is key to visual generation. *arXiv preprint arXiv:2310.05737*, 2023.
- [63] L. Zhang, A. Rao, and M. Agrawala. Adding conditional control to text-to-image diffusion models. In *Proceedings of the IEEE/CVF International Conference on Computer Vision*, pages 3836–3847, 2023.
- [64] R. Zhang, P. Isola, A. A. Efros, E. Shechtman, and O. Wang. The unreasonable effectiveness of deep features as a perceptual metric. In *Proceedings of the IEEE conference on computer vision and pattern recognition*, pages 586–595, 2018.
- [65] S. Zhang, X. Yang, Y. Feng, C. Qin, C.-C. Chen, N. Yu, Z. Chen, H. Wang, S. Savarese, S. Ermon, et al. Hive: Harnessing human feedback for instructional visual editing. In *Proceedings of the IEEE/CVF Conference on Computer Vision and Pattern Recognition*, pages 9026–9036, 2024.
- [66] Z. Zhang, L. Han, A. Ghosh, D. N. Metaxas, and J. Ren. Sine: Single image editing with text-to-image diffusion models. In *Proceedings of the IEEE/CVF Conference on Computer Vision and Pattern Recognition*, pages 6027–6037, 2023.

A Appendix

In this supplementary material, we first present an ablation study of our proposed methods, Regeneration and VARIN. Subsequently, we discuss a variation of VARIN editing, referred to as only target editing.

B Regeneration Algorithm

Algorithm 4 Editing by Regeneration

Input: Source image I_{src} , text prompt c_{tgt}

1: $r_1, r_2, \dots, r_K \leftarrow \mathcal{E}_{\text{VAR}}(I_{\text{src}})$

2: **for** t from s to K **do**

▷ s is starting regeneration scale

3: $\tilde{r}_t \sim p_\theta(\cdot | r_{<t}, c_{\text{tgt}})$

▷ Sampling using target prompt and token maps of previous scale

4: **end for**

5: $I_{\text{tgt}} \leftarrow \mathcal{D}_{\text{VAR}}(r_1, \dots, r_{s-1}, \tilde{r}_s, \dots, \tilde{r}_K)$

Output: I_{tgt}

C Ablation

In this section, we provide ablation details for our method VARIN and Regeneration. First, we examine the ablation study on the initial step of editing for the baseline Regeneration method. Finally, we do ablation on VARIN hyperparameter τ to indicate the importance of this hyperparameter in controlling how much information retains from the source images.

C.1 Regeneration

For the Regeneration method, we preserve the first few scales (from $s = 0$ to $s = 6$ or $s = 7$) and generate the remaining scales using the target prompt. As shown in Table 3, increasing the starting editing scale s leads to poorer performance on editing alignment metrics, such as structure distance and CLIP similarity, while improving performance on background preservation metrics. For qualitative results, refer to Figure 6. When $s = 0$, Regeneration behaves as a standard text-to-image generation process. However, when $s \geq 9$, the output image closely resembles the source image and, in some cases, fails to align with the provided target prompt (as illustrated in the first and second rows of Figure 6). On the other hand, with smaller scales $s \leq 5$, preserving the background from the original image becomes significantly challenging. Therefore, for editing tasks, the most effective scale to begin editing is within the range of $s = 6$ to $s = 8$.

Regeneration	Structure	CLIP Similarity		Background Preservation			
Begin Step	Distance $\times 10^3$ ↓	Whole ↑	Edited ↑	PSNR ↑	LPIPS $\times 10^3$ ↓	MSE $\times 10^4$ ↓	SSIM $\times 10^2$ ↑
$s = 6$	42.85	26.83	23.11	19.21	166.03	171.18	68.93
$s = 7$	33.70	26.08	22.57	20.49	137.00	133.17	70.79
$s = 8$	25.56	24.65	21.13	20.45	106.50	95.90	73.31

Table 3: Ablation on beginning step to edit for method Regeneration. Similar to observation from Figure 6, as s increases, the target alignment becomes worse while the background preservation is better. The recommended scale s is 6, based on qualitative result.

C.2 VARIN

Observing the qualitative and quantitative results of the Regeneration technique, we select the beginning editing scale $s = 6$. As mentioned in main paper, τ in Algorithm 1 also controls the retention of source information in the inverse noise n_t . As τ increases, the output image preserves the background more effectively (refer to Figure 7). Without τ , controlling the editing process becomes challenging, as inverse noise contains greater uncertainty about the source information, making it

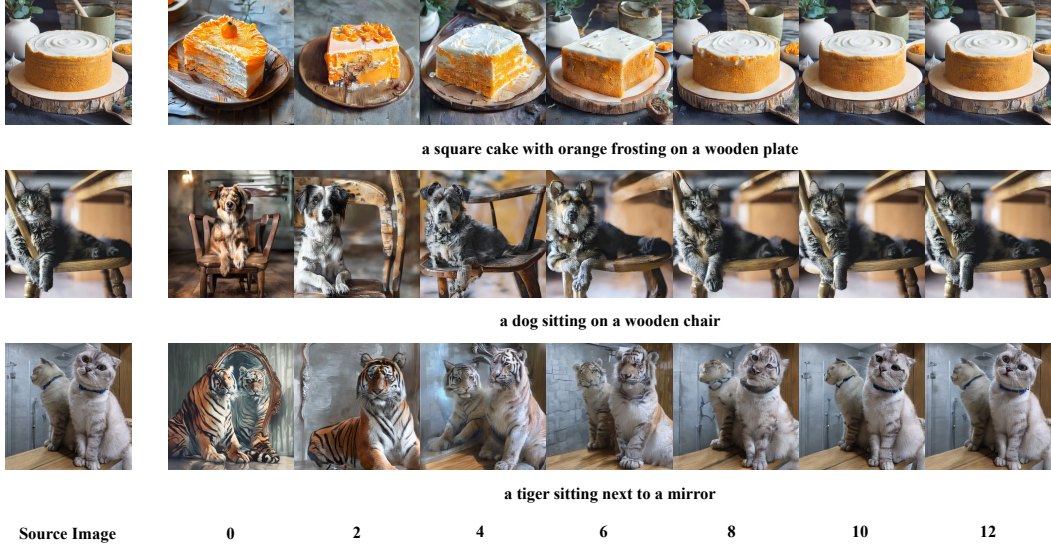


Figure 6: Ablation of Regeneration on beginning scale for editing s . We can see that as s increases, the edited image are more like the source image. For small s , the edited image is too different from the source image. Therefore, the best s for editing is around 6 to 8

more sensitive and less suitable for editing controllability. Since the hyperparameter τ is crucial for editing, we perform an ablation study on it in Table 4. Our findings indicate that τ values between 14 and 20 produce the best visual editing results.

VARIN	Structure	CLIP Similarity		Background Preservation			
τ	Distance $\times 10^3 \downarrow$	Whole \uparrow	Edited \uparrow	PSNR \uparrow	LPIPS $\times 10^3 \downarrow$	MSE $\times 10^4 \downarrow$	SSIM $\times 10^2 \uparrow$
14	19.21	25.73	22.12	23.97	74.23	68.49	82.26
16	14.33	25.32	21.72	25.49	60.87	48.97	84.34
18	11.46	25.05	21.49	26.54	54.04	38.33	85.39
20	9.85	24.79	21.28	27.30	50.28	31.78	85.96

Table 4: Ablation on value τ .

D Gumbel Truncation Sampling

For the Gumbel truncation algorithm [25], we provide the detailed algorithm in Algorithm 5.

Algorithm 5 GumbelTrunc

Input: location ϕ , threshold T

1: $u \sim \text{Uniform}(0, 1)$

Return: $\phi - \log(\exp(\phi - T) - \log u)$

E Editing using Only Target Prompt

In this section, we discuss the only target prompt VARIN, a variant of source-target VARIN in the main paper. In this editing algorithm, we only use target prompt c_{tgt} for both noise extraction and editing. First, we extract a set of inverse noises using the target prompt. This extracted noise set can then be used to perform the editing process, as shown in Algorithm 6. For this algorithm, qualitative results are provided in Figure 8, demonstrating that the source-target VARIN performs well on the

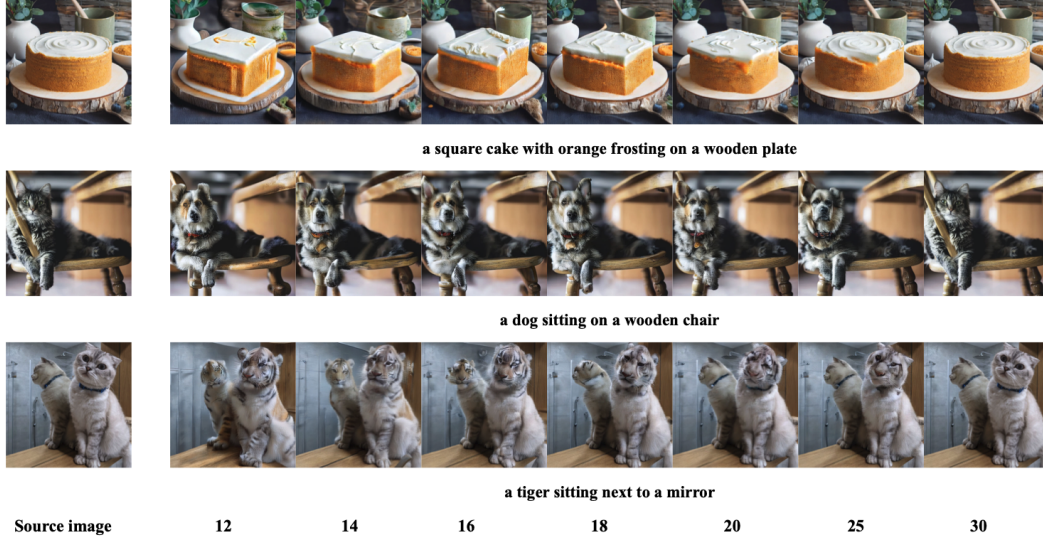


Figure 7: Qualitative result for ablation of τ for VARIN.

editing task. It is worth noting that for only target VARIN, the effective τ value is lower, typically between 10 and 14. In Table 5, we provide the ablation on τ for only target VARIN editing method.

Algorithm 6 Editing by target VARIN

Regeneration:

```

1:  $r_1, r_2, \dots, r_K \leftarrow \mathcal{E}_{\text{VAR}}(I_{\text{tgt}})$ 
2:  $n_1, n_2, \dots, n_K \leftarrow \text{VARIN}((r_1, r_2, \dots, r_K), c_{\text{tgt}})$ 
3: for  $t$  from  $s$  to  $K$  do
4:    $p_t \leftarrow p_{\theta}(r_t | r_{<t}, c_{\text{tgt}})$ 
5:    $g \sim \text{Gumbel}(0, I)$ 
6:    $q_t = p_t + (1 - \lambda) \cdot g + \lambda \cdot n_t$ 
7:    $r_t = \text{argmax}(q_t)$ 
8: end for
9:  $I_{\text{tgt}} \leftarrow \mathcal{D}_{\text{VAR}}(r_1, r_2, \dots, r_K)$ 
10: Return  $I_{\text{tgt}}$ .

```

$\triangleright s$ is the scale we start editing
 $\triangleright p_t$ is log probability

VARIN	Structure	CLIP Similarity		Background Preservation			
τ	Distance $\times 10^3 \downarrow$	Whole \uparrow	Edited \uparrow	PSNR \uparrow	LPIPS $\times 10^3 \downarrow$	MSE $\times 10^4 \downarrow$	SSIM $\times 10^2 \uparrow$
8	15.00	25.54	21.96	25.34	62.62	50.81	83.96
10	11.76	25.17	21.63	26.59	54.45	38.04	85.30
12	9.91	24.93	21.37	27.41	50.38	31.35	85.93
14	8.84	24.74	21.23	27.86	48.19	28.32	86.26

Table 5: Ablation on value τ of VARIN. As the τ increases, the edited image is more like the source image and preserve background better

F More Qualitative Comparison

See Figure 9, Figure 10, and Figure 12.

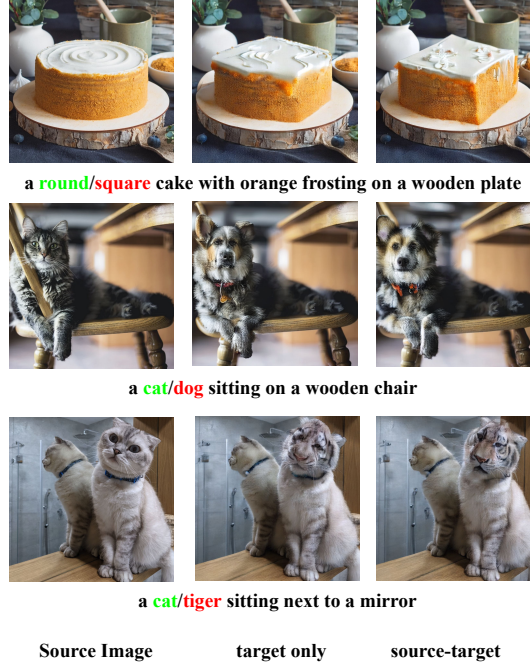


Figure 8: The first column is source image. The second column is target VARIN Algorithm 6, and the third column is source-target VARIN Algorithm 3. The green and red color texts are source and target prompt, correspondingly.

	DDPM-Inv	DICE	VARIN
Visualization quality	35.89%	15.89%	48.24%
Agreement to the editing prompt	52.35%	41.76%	64.71%

Table 6: User Study conducting on 25 people and 10 images.

G Limitation

Here we demonstrate one of the failure case that serves the limitation of our proposed method. As demonstrated in Figure 12, our method may fail in cases involving large pose or structural changes, or complex interactions that require such changes. These scenarios can challenge the model’s ability to preserve consistency and produce realistic edits.



Figure 9: Editing results on complex scene involves two objects.

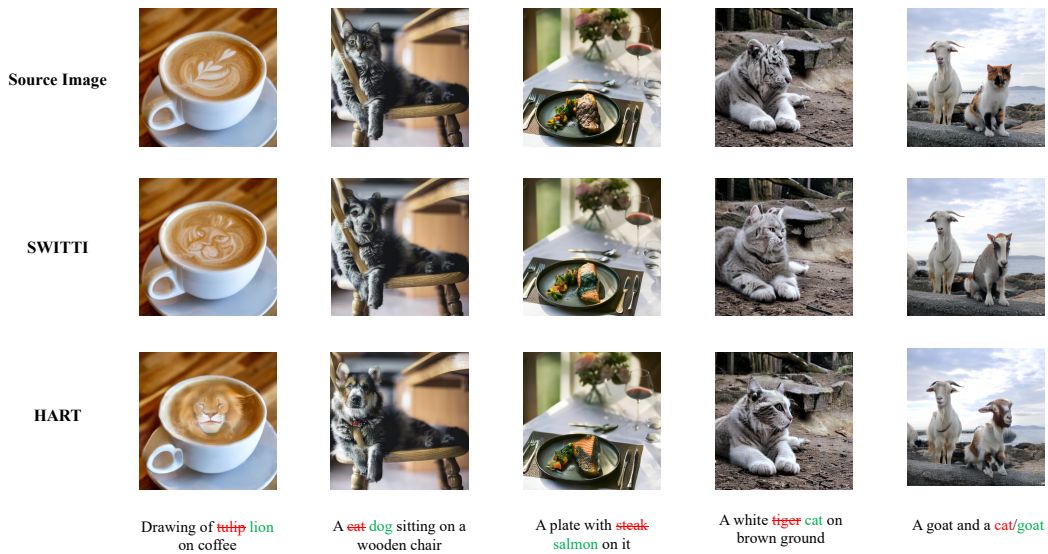


Figure 10: Extending VARIN to different architectures and base models.

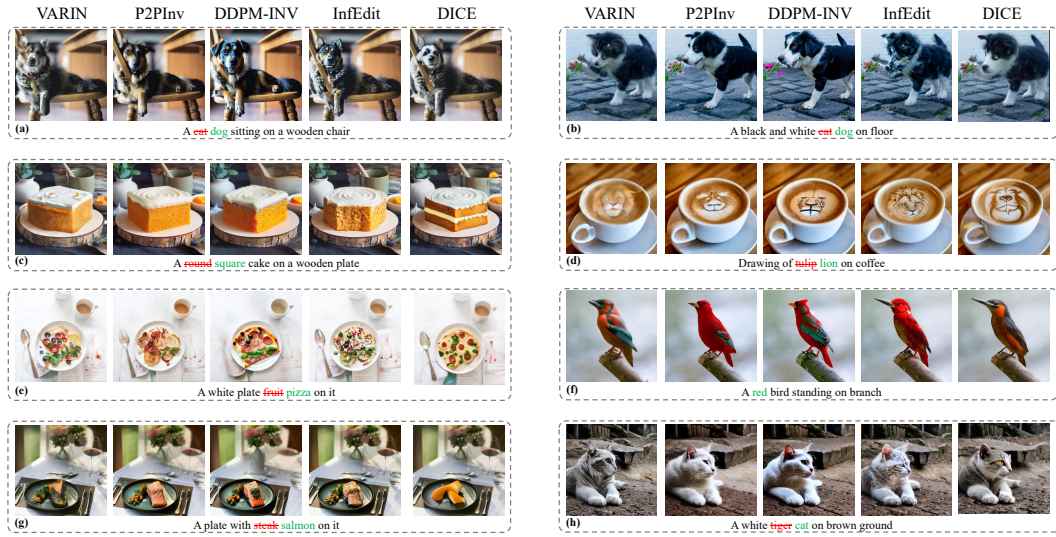


Figure 11: Comparing VARIN with different methods.

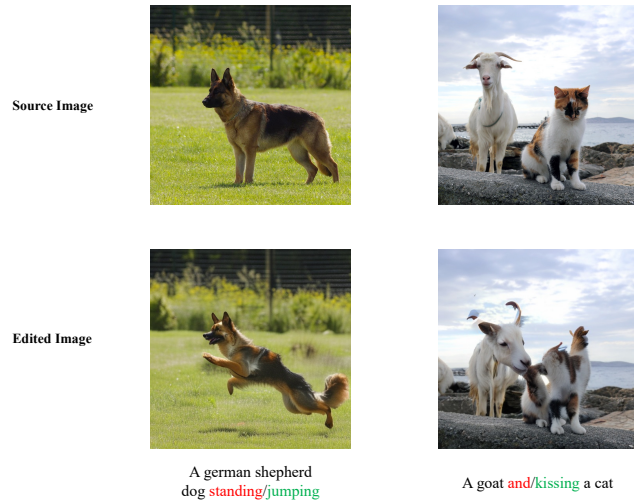


Figure 12: Failure cases: large movement and complex interaction between object